

Landscape features and urban heat island: episodic analyses during the dry season in a city of the Pre-Amazon region of Mato Grosso (Brazil)

Características paisagísticas e ilha de calor urbana: análises episódicas durante o período de estiagem em uma cidade da Pré-Amazônia Matrogrossense (Brasil)

Luis Flávio de Araújo

Universidade Estadual Paulista (Unesp),
Faculdade de Ciências e Tecnologia,
Presidente Prudente, São Paulo, Brasil



Margarete Amorim

Universidade Estadual Paulista, Faculdade
de Ciências e Tecnologia (Unesp),
Presidente Prudente, Brasil

Vincent Dubreuil

Departamento de Geografia, Université
Rennes II, Rennes, França

ABSTRACT

Research Purpose: This study aims to analyze the urban heat island in the city of Sinop (State of Mato Grosso, Brazil), based on three characteristic episodes of the dry season. The analysis focuses on the spatialization of temperature and the intensity of the phenomenon, as well as its association with landscape features.

Methodology: The analysis of the urban heat island was grounded in the Urban Climate System and the technical-methodological framework for investigating the phenomenon in medium and small-sized cities. Urban and rural landscape aspects were examined based on the adaptation of Local Climate Zones and the measurement of nighttime air temperature through mobile transects and fixed points. The data were processed and analyzed using statistical association techniques and multicriteria linear regression modeling, in order to predict the spatial distribution of air temperature and the intensity of the heat island.

Findings: The analyses highlight the influence of landscape features, physical elements, and urban spatial organization on temperature distribution and the formation of the heat island. They reinforce the mitigating role of vegetation and the greater heating in densely built areas, and also point to the influence of seasonality and regional atmospheric conditions on local thermal variation.

Originality/Value: The results highlight the effects of changes in local climatic aspects resulting from the reoccupation of the Pre-Amazon region of Mato Grosso through urban development and agricultural activities, in the generation and spatial distribution of phenomena such as the urban heat island. Furthermore, the study demonstrates the applicability of multicriteria modeling in understanding the spatial pattern of the phenomenon and its influencing factors, and emphasizes the importance of comprehensive analyses within the same seasonal period for a more accurate interpretation and the effective indication of mitigation and adaptation strategies.

Keywords: Urban climate; Landscape features; Multicriteria modeling; Tropical city.

RESUMO

Objetivo da Investigação: O presente artigo visa analisar a ilha de calor na cidade de Sinop (estado de Mato Grosso, Brasil), com base em três episódios característicos do período seco. A análise se concentra na espacialização da temperatura e da intensidade do fenômeno, assim como em sua associação com as características da paisagem.

Metodologia: A análise da ilha de calor foi fundamentada no Sistema Clima Urbano e no roteiro técnico-metodológico de investigação do fenômeno em cidades médias e pequenas. Dessa forma, foram verificados os aspectos paisagísticos urbanos e rurais a partir da adaptação das *Local Climate Zones* e da aferição da temperatura noturna do ar por meio de transectos móveis e pontos fixos. Os dados foram processados e analisados com base em técnicas estatísticas de associação e na utilização da modelagem pautada na regressão linear multicritério, a fim de prever a espacialização da temperatura do ar e da intensidade da ilha de calor.

Resultados: As análises evidenciam a influência da paisagem, dos elementos físicos e da organização urbana na distribuição da temperatura e na formação da ilha de calor. Reforçam o papel atenuante da vegetação e o maior aquecimento das áreas densamente construídas, além de apontarem a influência da sazonalidade e das condições atmosféricas regionais na variação térmica local.

Originalidade/Valor: Evidenciam-se os efeitos das alterações nos aspectos climáticos locais, decorrentes da reocupação da Pré-Amazônia Matrogrossense por meio da produção da cidade e das atividades agrícolas, na geração e espacialização de fenômenos como a ilha de calor. Destaca-se, ainda, a aplicabilidade da modelagem multicritério na compreensão do padrão espacial do fenômeno e de seus fatores de influência, além da importância de análises abrangentes dentro de um mesmo período sazonal para uma interpretação mais precisa e indicação eficaz de estratégias de mitigação e adaptação.

Palavras-chave: Clima urbano; Aspectos paisagísticos; Modelagem multicritério; Cidade tropical.

1. Introduction

The spatial production guided by socioeconomic contexts and logics gives rise to distinct landscapes and elements capable of altering natural mechanisms, such as water and energy balances, turbulent flows, among others (Oke et al., 2017). Such changes may be prolonged or permanent in the case of urban spaces, or they may exhibit a certain seasonality, which is related to the annual agricultural production practices carried out in the surroundings of the urban fabric (Stewart, 2011).

Cities, as symbols of radical human interference with nature, are characterized by a lack of vegetation, high building density, impervious surfaces, and features such as surface roughness. These characteristics enable changes in energy exchanges between the surface and the atmosphere and, consequently, in the components of the local climate, giving rise to the urban climate (Monteiro, 1975; Gartland, 2010; Oke et al., 2017; Amorim, 2020).

The urban heat island (UHI) is defined as a numerically positive alteration in the thermal field of cities compared to the rural environment (Fernández García, 1996; Gartland, 2010; Oke et al., 2017), serving as an example of the capacity of human activities to modify natural mechanisms. This is a potential problem for the population residing in these spaces, who perceive it through thermal discomfort, cardiorespiratory diseases, and floods, among others (Monteiro, 1975; Zheng et al., 2018). The segment of the population lacking the financial means to adequately cope with these issues is the most severely affected.

In the Brazilian context, case studies aimed at analyzing the impact of human activities on the local climate have gained strength since the 1970s, especially following Monteiro's (1975) proposal of the Urban Climate System (SCU, from the Portuguese acronym Sistema Clima Urbano). Monteiro introduced theoretical and methodological perspectives to understand the urban climate and heat islands, including the relationship between social and natural phenomena, as exemplified in studies by Amorim et al. (2021) and Ortiz Porangaba et al. (2021).

In the context of Amazonian cities, studies on urban climate remain limited and are mostly focused on large cities and state capitals, such as Manaus, Belém, and Porto Velho (Dubreuil et al., 2024). Research showing small and medium-sized cities is more recent and can be exemplified by the studies of Aleixo et al. (2021) on Uarini (a small city in the state of Amazonas) and Almeida Filho, Aleixo, and Silva Neto (2022) on Coari (a medium-sized city in the same state). Both cities are located within the dense Brazilian Amazon rainforest and exhibit thermal differences of up to 6 °C between urban and rural environments during the nighttime period of the dry season. Furthermore, Dubreuil et al. (2024) analyzed small and medium-sized cities on the pioneer front of the southern Amazon in Mato Grosso (Vera, Alta Floresta, Sorriso, and Sinop), which illustrate the intense transformation of the former tropical forest into young cities (most founded after 1974) driven by commodity-based agriculture. These areas present average monthly hourly temperature differences exceeding 3 °C between urban and rural zones.

It is noteworthy that the analysis of heat islands has used techniques for measuring the air temperature since its origin, such as the fixed stations technique, which consists of sensors fixed in locations of relevant interest for the research; and mobile transects, which consists of measuring sensors in motion on a given path. Such techniques

have certain restrictions, such as the low spatial amplitude of fixed points and the specificity of episodic results of mobile transects (Oke et al., 2017). The spatial restriction can be overcome with the use of geostatistical techniques that allow for advancement and new approaches in investigations (Foissard et al., 2019; Amorim et al., 2015; Yin et al., 2018).

Thus, the spatial modeling of the heat island, which consists of statistical estimation through linear regression of temperature or intensity values for points in the study area where it was not possible to obtain records from the values collected in situ (Foissard et al., 2019; Amorim, 2020), is an important analytical tool, presenting relevant results in tropical areas, as observed by Amorim et al. (2015), Dorigon and Amorim (2020), and Ortiz Porangaba et al. (2021), among others.

Alongside such techniques aimed at the spatialization of the phenomenon, the importance of its qualitative analysis is also highlighted, which can be assessed through intensity. Intensity comprises measuring the thermal difference between urban and rural areas (Oke, 1987), the magnitude of the heat island, and the characterization of the areas comprising the study object (Stewart and Oke, 2012).

Regarding the classification of UHI characteristics, Fernández García (1996) proposed the following magnitudes: weak ($0\text{ }^{\circ}\text{C}-2\text{ }^{\circ}\text{C}$), moderate ($2\text{ }^{\circ}\text{C}-4\text{ }^{\circ}\text{C}$), strong ($4\text{ }^{\circ}\text{C}-6\text{ }^{\circ}\text{C}$), and very strong ($>6\text{ }^{\circ}\text{C}$). Amorim (2020) further complemented this intensity-based analysis by introducing the concept of the ‘coolness island,’ which refers to a portion of the urban space that is less heated than its rural surroundings (magnitude values below $0\text{ }^{\circ}\text{C}$).

The spatial qualification of the study area can be carried out based on its landscape and built characteristics by using the Local Climate Zone (LCZ) classification system proposed by Stewart (2011). Among other aspects, this system offers the advantage of providing a globally applicable framework, a ‘universal language’, for describing urban and rural landscapes, while also overcoming the notion of a generic rural space by distinguishing rural areas that may influence local climate elements in different ways.

Therefore, based on the continuous densification of Brazilian cities, on the potential problems arising from the influence of socioeconomic activities on the characteristics of the local climate, and on the constant changes in the natural landscape, the present study aims to analyze the heat island present in the city of Sinop (state of Mato Grosso, Brazil) in three characteristic episodes of its drought period through the spatialization of temperature and heat island intensity and its association with landscape characteristics. To this end, the urban and rural spaces were characterized, the air temperature was measured, and the results were modeled and statistically validated.

1.1. Study area

The municipality of Sinop is located in the northern region of the state of Mato Grosso (Brazil), between 11° and 13° south latitude and 55° and 56° west longitude (Fig. 1). It covers a total area of $3,941.958\text{ km}^2$, of which approximately 1.7% (65 km^2) corresponds to the urban area, where a population of 196,312 inhabitants is concentrated, according to the Brazilian Institute of Geography and Statistics (IBGE, 2022).

As Sinop is inserted in the geomorphological unit of the Planalto dos Parecis, which is characterized by homogeneous altimetry and a well-developed drainage network (Brasil, 1980), its aspect physical setting enabled the implementation of a rectilinear urban layout, with forest fragments throughout the urban fabric.

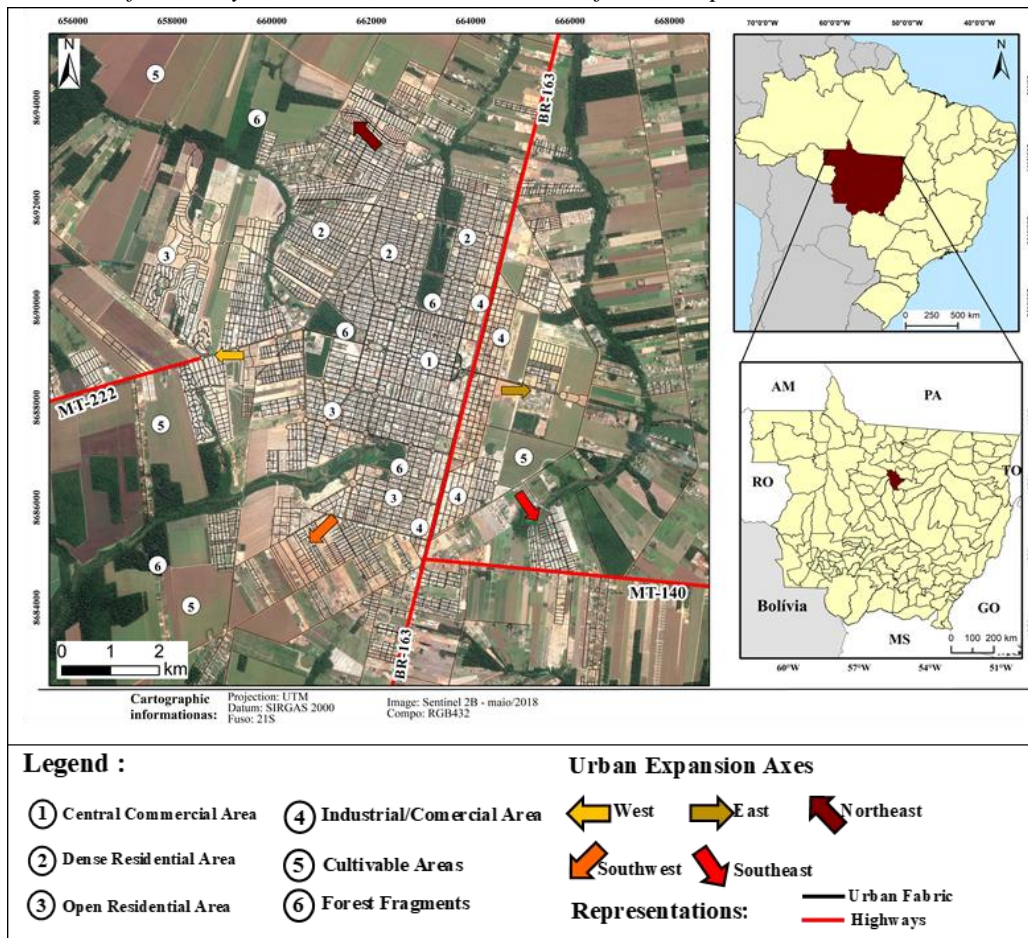
In the climatic context, based on the Köppen climate classification to define the annual climate types (ACT) and their frequency, Dubreuil et al. (2018) state that the area exhibits characteristics of the Aw type, characterized by a hot climate with summer rainfall and a dry winter season, with maximum precipitation occurring between December and February.

The formation and consolidation of the urban space was conceived by the colonizer SINOP (Real Estate Society of Northwestern Paraná, acronym in Portuguese) through government programs for the 'reoccupation' of the Legal Amazon and integration of these areas into the national economy, mainly during the 1970s. To this end, the legal instruments used were the implementation of infrastructure, such as the opening of the BR-163 highway and the facilitation of the distribution of land along federal highways; and stimulus to agribusiness as the main justifications for a strong presence of grain crop production and private colonization projects in this region of the country (Becker, 2001).

In view of this scenario, the company began implementing the urban plan in 1974 by establishing functional blocks (commercial, residential, service, and industrial), which served to guide the allocation of newcomers, consolidate the urban fabric, and inhibit the illegal occupation of lots.

As a result of such strategies, Sinop underwent an accelerated reoccupation of space that favored housing, pastures, and cultivated fields over the original vegetation, as highlighted by Clairay and Dubreuil (2002) and Dubreuil et al. (2003). This process, combined with the national economic direction for the production and sale of commodities from 1988 onwards, enabled the consolidation of the area with well-defined landscape characteristics both in urban and rural areas, as well as a latent urban expansion (Fig. 1).

Figure 1
Location of the study area and main uses and axes of urban expansion



Source: Sentinel 2B, 05/07/2018, color composite of RGB 432. IBGE, 2022.

2. Methodological procedures

This research is based on the Urban Climate System (SCU) proposed by Monteiro (1975) and on the technical-methodological framework for analyzing heat islands in medium and small cities developed by Amorim (2020).

The spatialization of the heat islands was elaborated through models that resulted from the application of multiple linear regression, which allows the prediction of values of a certain variable based on the knowledge of the values of other variables (Levin, 1977). For the purpose of measuring heat islands, this technique enables to predict the variation in air temperature (independent variable) from its correlation with the factors that comprise the study area (dependent variables), allowing the rational extrapolation of the data and connections found at sampling points to describe the occurrence of the phenomenon in the selected area.

The methodology applied, detailed in the following subsections, were described by Amorim (2020) and adapted from the original proposal by Foissard (2015) and Amorim et al. (2015). Most of the processes are executed in the software IDRISI®.

The generated models refer to three nocturnal episodes representative of the dry period in the study area,

characterized by stable atmospheric conditions, high air temperatures, and low relative humidity records throughout the days (September 18, 2020; July 20, 2023; and September 24, 2023). The dependent variables used include factors such as (a) the properties and landscape characteristics within the analytical scope (LCZ); (b) urban spatial organization (distance from the city center and distance from vegetation); and (c) physical elements (vegetation characteristics through the Normalized Difference Vegetation Index – NDVI). These variables were initially selected based on Foissard et al. (2019), Dorigon and Amorim (2019), Amorim (2020), and Ortiz Porangaba et al. (2021), and subsequently validated through statistical parameters.

2.1. Landscape properties and features

To qualify the surfaces and landscapes comprising the study area, a landscape classification system based on Local Climate Zones (LCZ) was adopted (Stewart, 2011). This system considers, among other elements, both natural and socially produced characteristics of spaces that influence the structure of the local climate. It defines LCZs as “regions of uniform surface cover, material, and human activity that span hundreds of meters to several kilometers in the horizontal plane” (Stewart and Oke, 2012), and which contribute to the formation of phenomena such as the urban heat island.

To perform this classification, construction and land cover characteristics were surveyed through visual interpretation of Sentinel-2 satellite imagery and Google Earth Pro® images obtained between March and October from 2020 to 2024. On-site visits were also conducted to refine and validate the assigned classes. These characteristics were surveyed based on the blocks of urban fabric and the homogenized elements of the rural surroundings, being adapted from the original proposal developed and presented by Cardoso and Amorim (2018).

Thus, nine LCZ classes and two subclasses were identified, with their classification and spatial distribution presented in Fig. 2. The characteristics of Sinop’s main LCZs are summarized in Table 1. These LCZs were also used as analytical units, as discussed in Section 3.

Figure 2

Spatialization of Sinop's landscape characteristics, mapped based on LCZs between 2020 and 2024

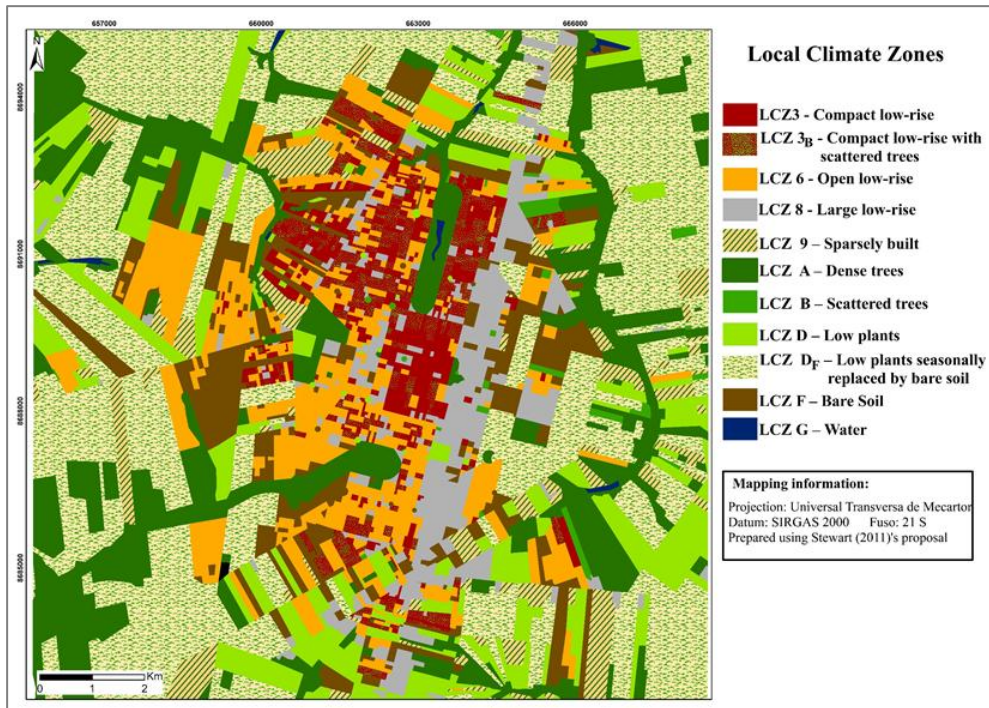


Table 1

Main LCZs identified in Sinop (MT), their characteristics, and examples of identification from aerial imagery

LCZs	Characteristics	Aerial view
3	Location: Concentrated in the central area of the city, being predominantly of commercial and residential use. Densely built-up areas, with a predominance of buildings with up to 3 floors. Presents paved land cover with few exceptions, with little or no arboreal vegetation; as well as plenty of heavy building materials (cement, stone, and bricks).	
3B	Location: Distributed in the northern portion of the urban fabric and with little presence in the south. Densely built up areas, with a predominance of buildings with up to 3 floors. Predominance of heavy construction materials and ceramic roofs, fiber cement, and zinc. It features paved land cover, as well as permeable areas (backyards and gardens), with the presence of spaced arboreal vegetation.	
6	Location: Distributed in the south, north, and west portions (expansion area). Spaced construction areas, with medium construction density. Small buildings, with heavy materials (brick, stone, and cement) and ceramic roofs. Scattered trees and permeable areas (backyards, gardens, and nonbuilt areas).	
8	Location: Predominantly distributed along the federal highway (industrial sector) and connecting road axles. Areas of elongated and small buildings of heavy materials and roofs with metallic structures and sheets of zinc or fiber cement. It may have permeable areas and trees, although paved areas predominates.	
A	Location: Fragments dispersed in the intra-urban and rural areas, being frequently associated with water courses. Densely wooded area, permeable and with or without ground vegetation.	
Df	Location: Predominant in the rural surroundings of Sinop, with patches within areas of urban expansion. Area seasonally occupied by ground vegetation or exposed soil. It does not present paved areas in large extensions, as well as buildings.	

Source: Aerial images taken from Google Earth Pro®. Developed by the authors (2025).

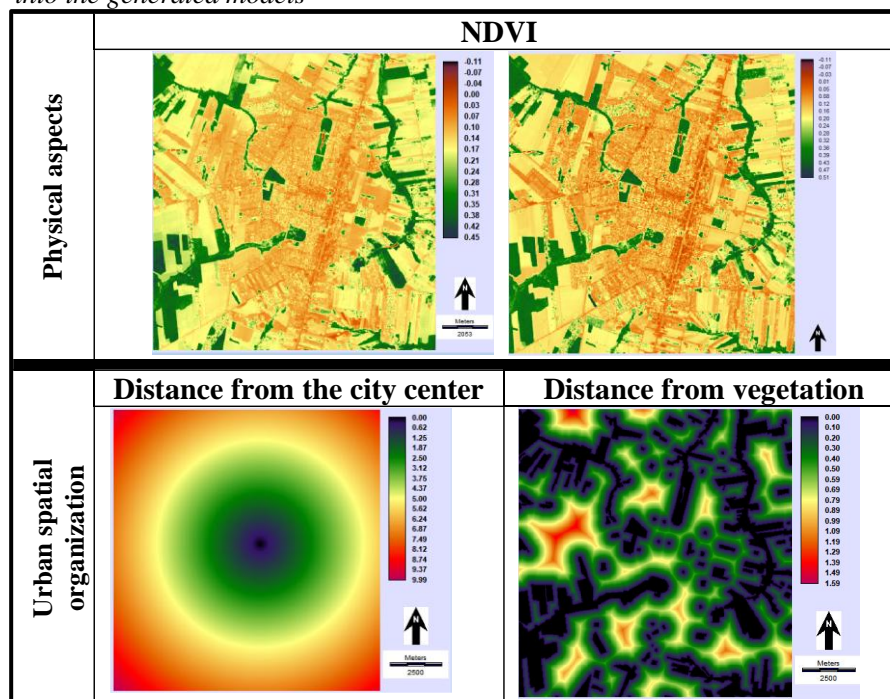
For the application of the landscape characteristics in the generated models, the LCZs were inserted in 8 classes, according to their similarities. Thus, the following classes were available for this research: C1 (LCZ 3), C2 (LCZ 3_B), C3 (LCZ 6), C4 (LCZ 8), C5 (LCZ 9), C6 (LCZ A + LCZ B), C7 (LCZ D), and C8 (LCZ D_F).

After reclassifying the land use categories, the number of pixels surrounding each measurement point was calculated using windows of different sizes, such as 3×3 pixels (90 m × 90 m), 5×5 (150 m × 150 m), and 7×7 (210 m × 210 m), until appropriate parameters were identified for statistically validating the relationships. This step is justified by Amorim et al. (2015, p. 38), who state that “[...] it is not initially known what the area of influence of land use on temperature measurements for each point” highlighting the need for testing multiple window sizes.

2.2. Landscape properties and features

In addition to the landscape characteristics represented by the LCZ classes and based on studies focused on the spatial modeling of urban heat islands, additional factors were incorporated into the models presented in this paper. These factors were grouped into two categories: (1) physical aspects, represented by NDVI, and (2) urban spatial organization, expressed as distances from key features such as the city center and vegetation (Fig. 3).

Figure 3
Information on physical aspects and urban spatial organization incorporated into the generated models



Data source: NDVI: USGS (2020; 2023).

To obtain NDVI values using IDRISI® software, bands 4 (Red) and 5 (Near Infrared) from Landsat 8/9 (OLI sensor) images dated 12 September 2020, 20 July 2023, and 22 September 2023 were used. The result, shown in Fig. 3, reveals that during the analyzed episodes, the highest vegetation indices were concentrated around the urban fabric and specific intra-urban locations, associated with forest fragments and watercourses. Within the urban fabric and cultivated areas, values ranged from -0.04 to 0.17, indicating a significant presence of exposed soil in the rural

surroundings.

The justification for adopting the variable ‘distance from the city center’ lies in the assumption that, given its constructive characteristics, the city center tends to be warmer than other intra-urban and rural areas, with a reduction in air temperature as one moves towards the rural environment due to the low density of construction in these areas. On the other hand, the use of distance from vegetation is based on the distribution pattern of temperature and heat island intensity, as verified by Araújo (2021). These elements are fundamental for the explanation of the models.

To obtain distance values in kilometers, buffers were generated around tree vegetation classes for the variable ‘distance from vegetation,’ and from a point selected in the central area of the city, based on the mobile transect collection points, for the variable ‘distance from the city center.’ Distance values for each measurement point were then extracted and analyzed for their relationship with temperature variation before being applied in the models. Both steps were performed using IDRISI® software.

2.3. Measurement of air temperature

As discussed above, despite presenting a time limitation, mobile transects allow for better detailing the spatialization of air temperature as a function of the landscape characteristics of the area. Oke et al. (2017) indicated that the total time traveled by the transects on the routes should not exceed one hour of execution, so that the thermal difference can be protected and analyzed in relation to the environment and not to the natural temperature variation, giving priority to performing this experiment at night.

The justification for performing this procedure at night lies in the fact that air temperatures do not express rapid changes during this period, allowing the collection of the first and last values within the same thermal range (Pitton, 1997; Amorim, 2005, 2020).

The routes were covered on 18 September 2020, 20 July 2023, and 24 September 2023 under stable atmospheric conditions, with clear skies and calm winds, using a vehicle equipped with a sensor traveling at an average speed of 25 km/h. Data collection began at 21:00 (local time) and lasted approximately 50 to 55 minutes. Air temperature was recorded at predetermined points spaced 200 meters apart, with the Avenza Maps® application used to control measurement locations for each survey episode, as described by Pinton et al. (2021).

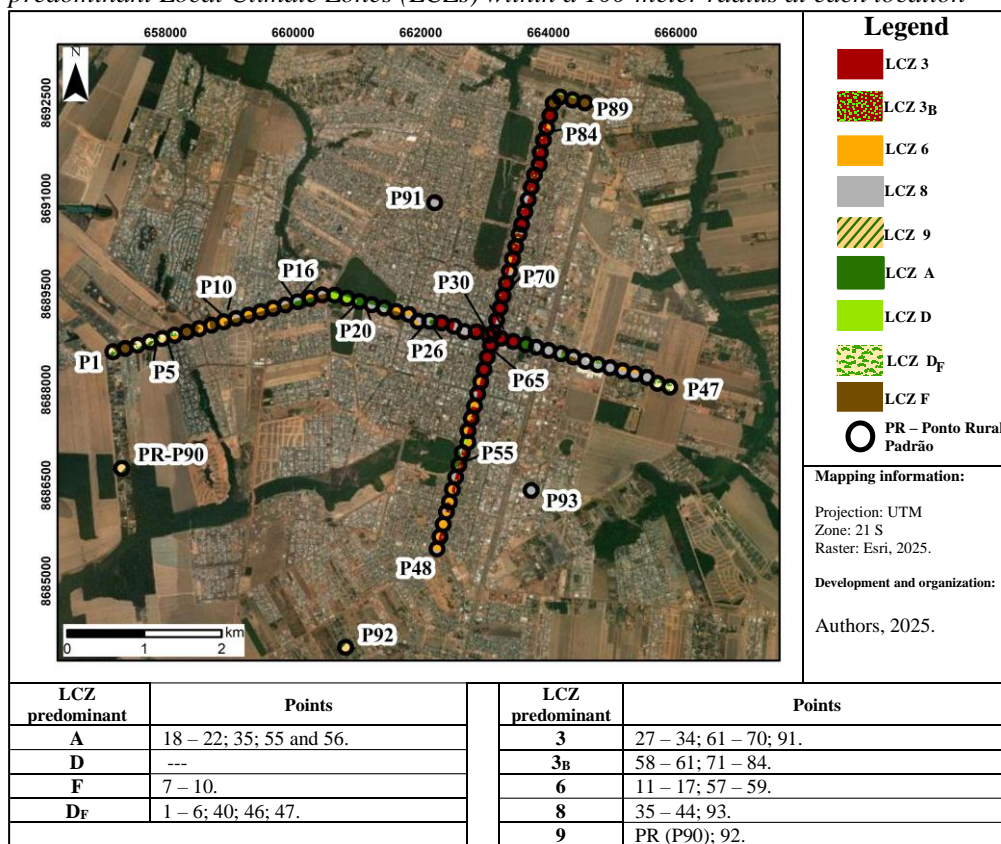
In order to encompass the specific LCZs of the study area, West-East and South-North routes were established (Fig. 4). The first route (W-E) passed through characteristic areas of rural use (LCZ D_F), urban expansion (LCZs 6, F), forest fragments (LCZ A), the commercial city center (LCZ 3), areas of “industrial use” (LCZ 8) and ended in rural areas close to watercourses.

The S-N route primarily took place in the intra-urban area, passing through areas with high building density without or with vegetation (LCZ 3 and 3B), an urban area in consolidation (LCZ 6 and F) and points of dense arboreal vegetation.

In addition to the mobile transect points, data recorded at 21:00 from three fixed stations were used, each equipped with specific instruments and located in distinct landscape contexts. A weather station (Davis Vantage Pro2), with an air temperature accuracy of $\pm 0.5\text{ }^{\circ}\text{C}$ and a resolution of $0.1\text{ }^{\circ}\text{C}$ (Davis Instruments, 2019), was installed in a rural area (LCZ 9) near a forest fragment and was designated as the standard rural point for further analysis (PR–P90, Fig. 4). TinyTag Ultra 2 data loggers, equipped with RS3 solar radiation shields, offering an accuracy of $\pm 0.5\text{ }^{\circ}\text{C}$ (within the $0\text{ }^{\circ}\text{C}$ – $50\text{ }^{\circ}\text{C}$ range) and a resolution of $0.01\text{ }^{\circ}\text{C}$, were installed at additional sites: one in a high-density residential area (LCZ 3), represented by P91 (Fig. 4); one in a rural–urban transition zone (P92); and another in an industrial use area (P93).

Figure 4

Routes of mobile transects, fixed and mobile air temperature collection points, and predominant Local Climate Zones (LCZs) within a 100-meter radius at each location



Source: Esri (2021).

2.4. Spatial Modeling: parameters for the selection of independent variables and model validation

The selection of independent variables included in the statistical models for the selected dates was based on the analysis of partial coefficients of determination for each characteristic in relation to air temperature, obtained through simple linear regression, as well as the correlation values between the variables and temperatures measured during the mobile transects, as illustrated in Fig. 5.

Figure 5

Coefficients of determination and correlation used as analytical parameters in the generation of the models

18 Sept. 2020			20 Jul. 2023			24 Sept. 2023		
R ² (%)	Variables	Temp	R ² (%)	Variables	Temp	R ² (%)	Variables	Temp
28	C1_97x97	0.53	11.5	C1_61x61	0.34	17	C6_81x81	-0.41
18	C6_97x97	-0.42	11	C6_81x81	-0.33	18	C8_3x3	-0.42
8	C3_97x97	0.28	27	Dist. centro	-0.52	32	Dist. centro	-0.57
2	C2_97x97	0.13	6.5	LST	-0.25			
25.6	C8_3x3	-0.49						
29	Dist. centro	-0.54						
3	Dist. vezt	0.17						
20.3	NDVI	-0.45						

Legend		
Landscape property classes: C1-LCZ 3 C2-LCZ 3 _B C3-LCZ 6 C4-LCZ 8 C5- LCZ 9 C6- LCZ A + LCZ B C7- LCZ D C8- LCZ D _F	Dist. centro: Distance from the city center	
	Dist. vezt = Distance from vegetation	
	NDVI = Normalized Difference Vegetation Index	Correlation strength
	LST =Land surface temperature	Very weak Weak Moderate

An analysis of Fig. 5 indicates that of the eight predictor variables related to the 09/18/2020 model, five presented a coefficient of determination above 10%: distance from the city center ($R^2 = 29\%$), NDVI ($R^2 = 20.3\%$), and the landscape classes C1_97x97 ($R^2 = 28\%$), C7_3x3 ($R^2 = 25.6\%$), and C5_97x97 ($R^2 = 18\%$). This result indicates that the factors that best explained the response variable were: the spatial organization associated with distance and landscape change relative to the city center; the characteristics of densely built-up areas (LCZ 3); and the presence of arboreal vegetation (C5/LCZs A and B) or cultivated areas, reinforcing the influence of human activities on local climate characteristics.

The other three predictor variables of this model presented R^2 values between 2% and 8%, with the landscape class C2_97x97 showing the lowest coefficient. However, as these variables exhibited correlations not only with air temperature, their inclusion in the model was essential, as they contributed to reducing residuals and improving the accuracy of the cartographic representation.

The constituent data of the models from July 18 and September 24, 2023, show similarities with the previous model, indicating the greatest influence on air temperature distribution from the distance to the city center (with R^2 values of 27% and 32%, respectively), as well as from landscape characteristics associated with densely built-up areas (C1), dense vegetation (C6), and rural land use (C8). Notably, the main difference between the two 2023 models and the one generated for 2020 lies in the reduction of explanatory variables, without compromising the

robustness of the models. This is a result of the intra-seasonal characteristics represented by each episode: the September 2020 model corresponds to prolonged drought conditions, distant from the rainy season; the July 2023 model reflects the early months of the dry period, which typically begins in May/June; and the September 2023 episode, in addition to being associated with atmospheric blocking typical of central Brazil's seasonal patterns, also represents the occurrence of a heatwave in the study area.

In general, when verifying the correlation of predictor variables that are significant to explain the variation in air temperature, there is an indication of the landscape properties that most influence the characteristics of the local climate, such as vegetated areas, especially those with high density, and densely built portions from the urban fabric.

When taking into account not only the individual participation of the elements in the influence of air temperature variation but also the interrelationship of factors, it was possible to identify the complexity that is typical of urban heat islands, in which the modification and composition of the landscape, together with atmospheric conditions, interfere with thermal characteristics at the local scale, reaffirming the need to apply analytical techniques such as spatial modeling for a better interpretation of this phenomenon.

From the selected predictor variables and the parameters aforementioned, multiple linear regression was applied. Thus, the formulas that mathematically describe the variation in air temperature as a function of landscape elements were obtained, with the results being subsequently specialized into maps using the software IDRISI®. The resulting formulas are shown below:

$$Tm(18_{09}) = 31.1044 + 0.0155 * C1_{97x97} - 0.2428 * C6_{97x97} - 0.2149 * C8_{3x3} + 0.0611 * C3_{97x97} - 0.2319 * Dist_{centro} - 10.4161 * NDVI + 0.1635 * Dist_{vegt} - 0.0067 * C2_{97x97} \quad (1)$$

$$Tm(20_{07}) = 39.932441 - 0.366187 * C6_{81x81} - 0.510517 * Dist_{centro} - 0.521505 * LST - 0.062871 * C1_{61x61} \quad (2)$$

$$Tm(24_{09}) = 28.633423 - 0.163035 * C6_{81x81} - 0.108497 * C8_{3x3} - 0.294596 * Dist_{centro} \quad (3)$$

Where :

$Tm(18_{09}/20_{07}/24_{09})$ = Modeled air temperature for September 18, 2020; July 20, 2023; and September 24, 2023;

$C1_{(97x97/61x61)}$ = class 1 (LCZ 3) values within 97x97 or 61x61 pixel window surrounding the sampling point;

$C2_{97x97}$ = class 2 (LCZ 3B) values within 97x97 pixel window surrounding the sampling point;

$C3_{97x97}$ = class 2 (LCZ 6) values within 97x97 pixel window surrounding the sampling point;

$C6_{(97x97/81x81)}$ = class 6 (LCZ A + B) values within 97x97 or 81x81 pixel window surrounding the sampling point;

$C8_{3x3}$ = class 8 (LCZ DF) values within 3x3 pixel window surrounding the sampling point;

$Dist_{centro}$ = distance from the city center;

$Dist_{vegt}$ = distance from vegetation;

NDVI = Normalized Difference Vegetation Index;

LST = Land Surface Temperature.

For the reliability analysis of the models obtained, analytical parameters such as Analysis of Variance (ANOVA), the F-test, the adjusted coefficient of determination (R^2_{adjusted}), and residual analysis were employed, all of which were calculated using Excel® software. Table 1 presents the aforementioned parameters for the models generated using air temperature and landscape characteristics of the study area.

Table 2

F-statistics, significance level (F), and adjusted coefficient of determination (R^2_{adjusted}) for the validation of the generated models

Date	F	F of significance	R^2_{adjusted}
18 Sep 2020	12.66	< 0.001	0.62
20 Jul 2023	23.7	< 0.001	0.51
24 Sep 2023	46.6	< 0.001	0.60

Based on the data shown in Table 1, it is noted that the values of F and F of significance, which are below $\alpha = 0.05$, enable to refute the null hypothesis (variations occurring at random) for the models, indicating the relationship of at least one predictor variable with the response variable and the significance of the models within the 95% range. Thus, by associating these results with those of R^2_{adjusted} , the models explain, respectively, 62%, 51% and 60% of the variation in air temperature as a function of landscape properties.

In order to refine the validation of the models, since the global validation was attested through the parameters presented above, the analysis of the residuals was carried out, that is, if there was distance or approximation between the adjusted (modeled) temperature and the measured temperature. For this purpose, the values of the modeled temperature were subtracted from the measured temperature and the result was presented through scatter plots prepared using the software Excel®.

It is pointed out that this qualitative analysis was based on 89 points of mobile transects (P1 to P89) and on four fixed points, PR-P90 (standard rural point), P91 (consolidated urban area), P92 (urban expansion area) and P93 (industrial area), totaling 93 points for verification.

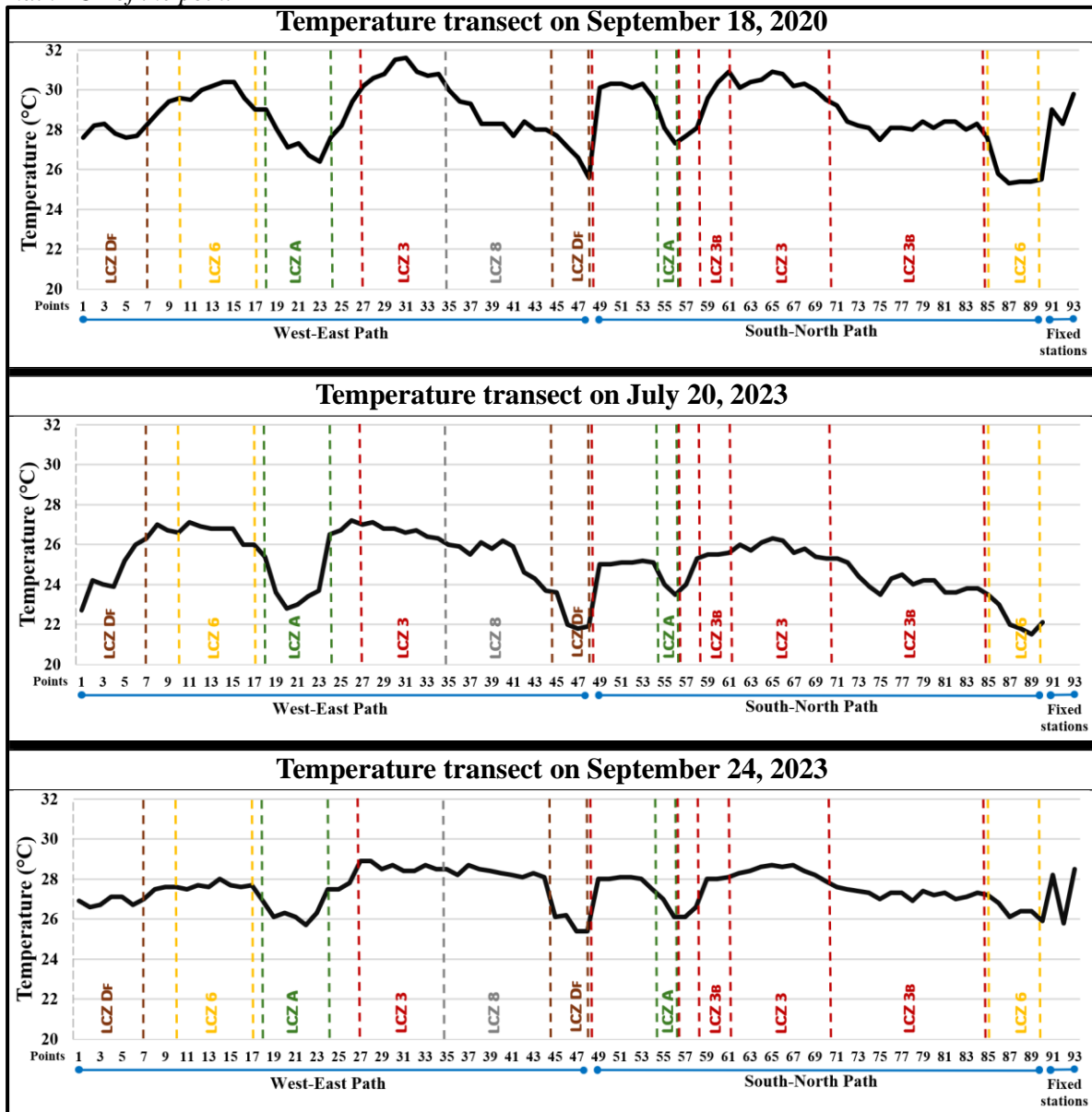
3. Results and discussion

3.1. Mobile measurements of the analyzed episodes

The data measured through mobile transects between 21:00 and 22:00 (local time) for September 18, 2020, July 20, 2023, and September 24, 2023, are shown in Fig. 6, allowing for a better initial understanding of the spatialization of the air temperature as a function of the building and landscape characteristics of the transects. These profiles, which represent the collection points on the abscissa axis and the air temperature on the ordinate axis, were prepared using Excel® software.

Figure 6

Spatialization of air temperature measured in the transects on September 11 and 18, 2020, between 21:00h and 22:00h. Horizontal lines indicate the thermal profile, while vertical dashed lines indicate the main LCZ of the point



The results shown in Figure 6 demonstrate a strong relationship between air temperature and the landscape features of Sinop, as evidenced by the following observations: greater thermal variation along the W–E transect due to the diversity of landscape characteristics; temperature reductions at locations with dense tree vegetation and their surroundings; a modest thermal difference between LCZs 3 and 3_B; and the association of higher temperatures with LCZ 3 points, as well as with LCZ 8 points when compared to vegetated areas, although LCZ 8 areas remain slightly cooler than those in LCZ 3.

These characteristics are supported by previous studies, such as those conducted by Dubreuil et al. (2003, 2010), Zavitoski (2018), Araújo et al. (2022). Moreover, they reinforce the relationship between local temperature and the

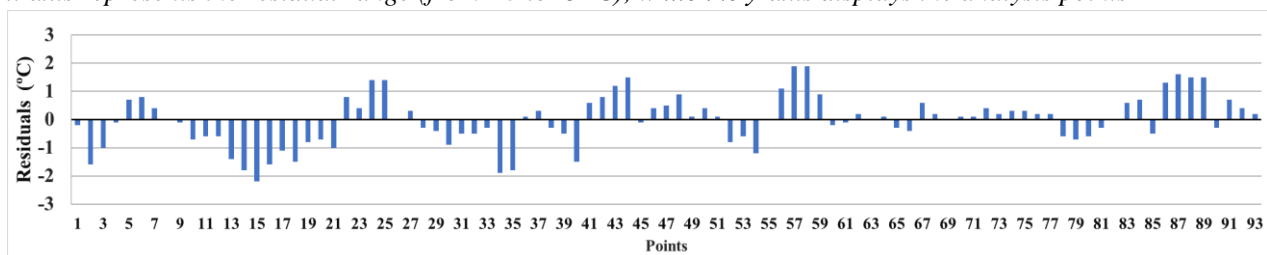
landscape features distributed across the city, thereby justifying the use of spatial modeling as a means of representing this reality, which is the central focus of this study.

3.2. The global validation of models and the analysis of residuals

The residuals for the model from 18 September 2020 (Fig. 7) ranged from -2.2 °C to 2.2 °C. Values exceeding ±2 °C, or close to this range, were observed at points P15, P57–P59, and P86–P89, which are characterized as urban expansion areas or transition zones to LCZ 3_B.

Figure 7

Spatial distribution of residuals by point for the punctual validation of the 18 September 2020 model results. The x-axis represents the residual range (from +3 to -3 °C), while the y-axis displays the analysis points



Points P24–P25, located near forest fragments in the western portion and in the transition to the urban area; P43–P44, characterized by LCZ 8; P63–P65, near dense arboreal vegetation and classified as LCZ 6; and P86–P89, falling within LCZs F and D, showed residual values ranging from 1 °C to 1.9 °C. Conversely, points P2–P3, with LCZ D_F characteristics; P13–P14 and P16–P18, representing areas of urban expansion with a predominance of LCZs 6 and F; P21–P35, located in LCZ A; P34, corresponding to a densely built area; P40, consisting of LCZs 8 and F; and P61, near dense arboreal vegetation and predominantly classified as LCZ 8, presented residual values ranging from -1 °C to -1.9 °C.

Based on the classification of residuals shown in Table 3, 72% of the points analyzed for validation presented values close to or equal to those measured, while 17% were underestimated and 11% overestimated. This fact also validates, on a more detailed scale, the results in confidence intervals.

Table 3

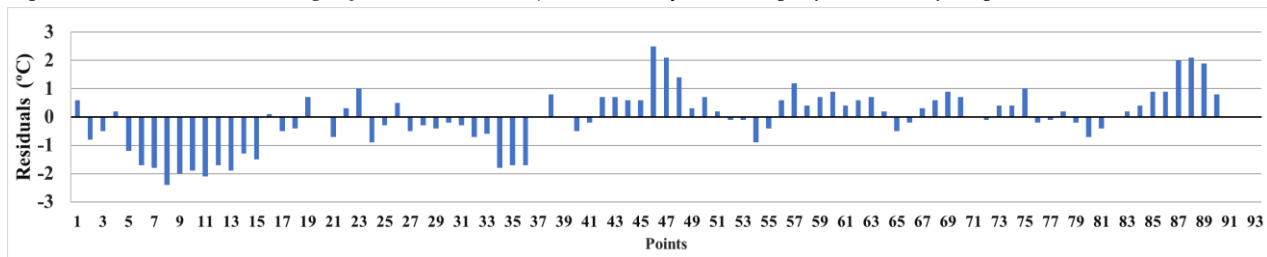
Qualitative analysis of point-based residuals obtained from the model for 18 September 2020

Measured and modeled air temperature difference classes	Number of points	Percentage	Model Results
Between -2°C e -3°C	2	2	Underestimated (17%)
Between -1°C e -2°C	15	15	
Between -1°C e 1°C	71	72	Equaled or approximated (72%)
Between 1° C e 2° C	10	10	Overestimated (11%)
Between 2° C e 3° C	1	1	

The residuals from the model generated for the 20 July 2023 episode (Fig. 8) show certain similarities in their distribution when compared to the previous model. The first observation concerns the similar range of residuals, as the present model shows values between the thresholds of 2.5 and -2.5. The second observation refers to the fact that the highest residuals, both positive and negative (ranging from -2.4 to 2.5), were associated with urban–rural transition areas (P8 to P12, P45–P47, and P86–P88), where the landscape features are more complex than in consolidated urban areas, indicating that their relationships may involve additional variables.

Figure 8

Spatial distribution of residuals by point for the punctual validation of the 20 July 2023 model results. The x-axis represents the residual range (from +3 to -3 °C), while the y-axis displays the analysis points



Another point of similarity between these first two models emerges from the qualitative analysis of the residuals (Table 4). For the 20 July 2023 model, approximately 77% of the residuals correspond to values that were equal to or close to those measured at the collection points. The remaining residuals were distributed as follows: 7% were overestimated (with differences ranging from 1.1 to above 2 °C), and 15% were underestimated (ranging from -1.1 to -2.5 °C). As previously mentioned, these processes of overestimation or underestimation of the modeled values originated from points located at the interface between rural and urban areas. In the thermal profiles obtained from the mobile transects, these points reveal abrupt changes in temperature that could not be fully captured by the model, without, however, compromising its explanatory capacity.

Table 4

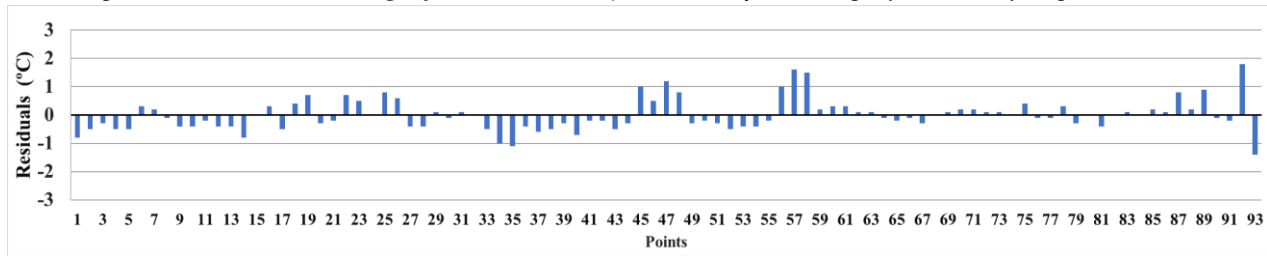
Qualitative analysis of point-based residuals obtained from the model for 20 July 2023

Measured and modeled air temperature difference classes	Number of points	Percentage	Model Results
Between -2°C e -3°C	2	2	Underestimated (15%)
Between -1°C e -2°C	12	13	
Between -1°C e 1°C	69	77	Equaled or approximated (77%)
Between 1° C e 2° C	4	4	Overestimated (7%)
Between 2° C e 3° C	3	3	

The residuals found for the model from 24 September 2023 (Fig. 9) differ from those of the two previous models. Initially, it is noted that the modeled data were closer to those measured by the mobile transects, with most residuals predominantly ranging between 0.8 and -0.8 °C. A few exceptions were observed, such as at point P92 (2.1 °C) and points P15–P16 and P47 (ranging between 1.4 and -1.2 °C).

Figure 9

Spatial distribution of residuals by point for the punctual validation of the 24 September 2023 model results. The x-axis represents the residual range (from +3 to -3 °C), while the y-axis displays the analysis points



Based on Table 5, it is observed that 94% of the modeled data were equal to or close to the original measurements, with only 4% being overestimated (ranging from 1.1 to 2 °C). A possible explanation for this outcome lies in the atmospheric conditions during the episode, which was under the influence of a blocking pattern and characterized as a heatwave. As a result, urban and rural temperatures were more similar (as observed in Fig. 6), except under specific conditions such as the presence of dense arboreal vegetation.

Table 5

Qualitative analysis of point-based residuals obtained from the model for 24 September 2023

Measured and modeled air temperature difference classes	Number of points	Percentage	Model Results
Between -2°C e -3°C	0	0	Underestimated (2%)
Between -1°C e -2°C	2	2	
Between -1°C e 1°C	87	94	Equaled or approximated (94%)
Between 1° C e 2° C	3	3	Overestimated (4%)
Between 2° C e 3° C	1	1	

The parameters presented above attest to the statistical significance of the models and, through the refined validation of the residuals, allow the identification of points classified as prolonged residuals—locations where, regardless of the influencing factors, the models fail to adequately explain the temperature values. These points mark the boundaries of model applicability and reliability. As an example, points P13 to P16, characterized by LCZs F and 6, and point P17, associated with LCZs 8 and F, showed underestimated temperature values and are thus identified as prolonged residuals.

Thus, starting from the validation of the models, temperature charts representing the spatialization of the urban heat island in Sinop were created through the characteristics of the modeled temperature and the intensity and magnitude of the UHI, with the latter being based on Fernández García (1996), for further analysis.

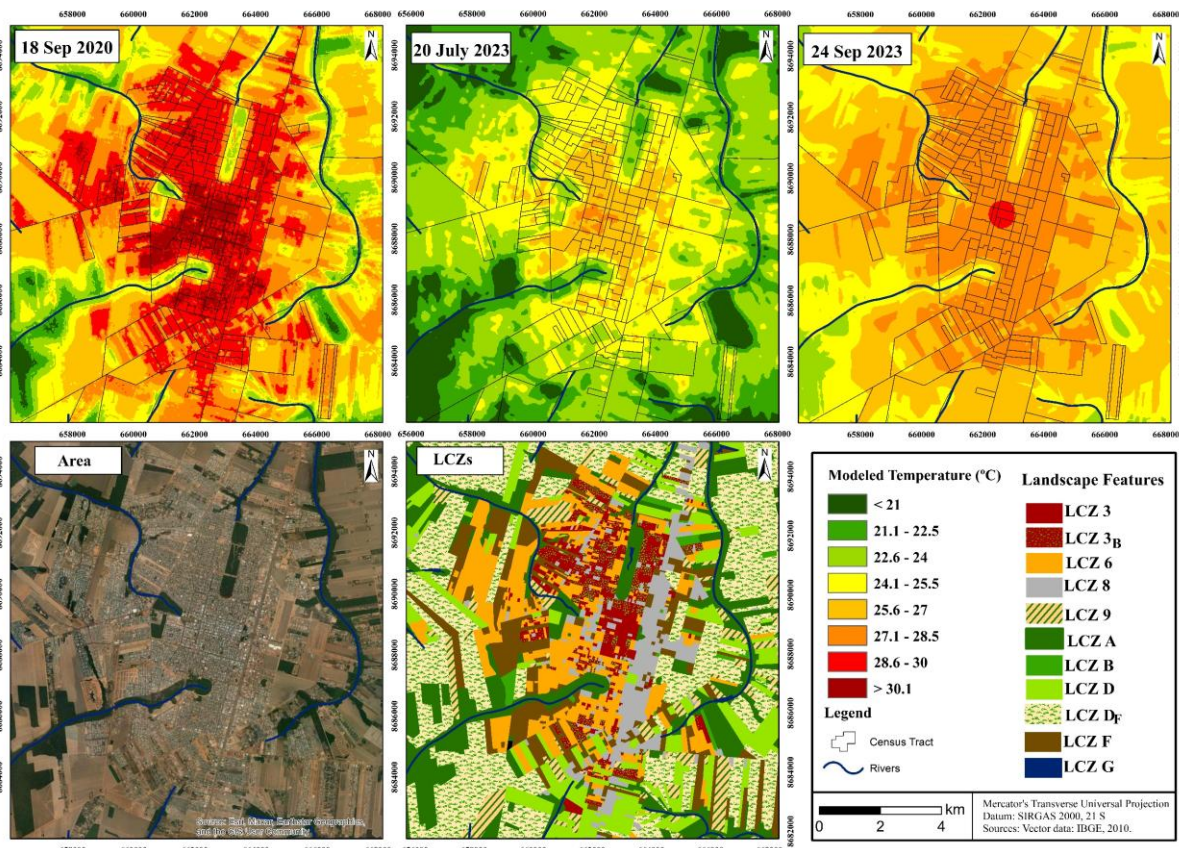
3.3. Spatial Representation of the Model Results

Given the validation of the models by the parameters presented above, the results were spatialized in two ways. First, air temperature was modeled to enable a more precise assessment of the results based on the residuals. Second, the intensity and magnitude of the urban heat island were spatialized, thereby qualifying the thermal differences and supporting the analysis of the relationship between landscape characteristics and air temperature.

Figure 10 presents the spatialization of the modeled air temperature for 18 September 2020, 20 July 2023, and 24 September 2023, at 21:00 (local time). A comparison between the dates initially reveals that each one exhibits a specific thermal gradient associated with its seasonal conditions. Nevertheless, it can be observed that the distribution of the modeled temperature values presents similarities across the episodes. Higher temperatures tend to concentrate in consolidated urban areas and zones of expansion, which are characterized by high building density and exposed soil. Conversely, lower temperature values are consistently found in areas with vegetation, particularly those located farther from the urban fabric.

Figure 10

Spatialization maps of the temperature modeled for 18 September 2020, 20 July 2023, and 24 September 2023 at 21:00 (local time), along with the corresponding Local Climate Zones (LCZs)



In the detailed analysis of the results presented in Fig. 10, it is observed that the thermal ranges < 20 °C, 21.1 °C–22.5 °C, and 22.6 °C–24 °C were restricted to areas of arboreal vegetation (LCZ A) and small portions of LCZ D_F near vegetation, which were concentrated in the southwestern portion of the temperature map. Values between 24.1 °C and 27 °C were associated with areas characterized by LCZ D_F.

The rural–urban transition zones showed temperature values ranging from 27.1 °C to 28.5 °C, indicating higher temperatures in intra-urban areas. Within the urban fabric, the thermal range of 28.6 °C to 30 °C predominated in LCZs 3_B and 8, while values above 30 °C were recorded in LCZs 3 and 6, particularly in the central-western portion.

For the episode of July 20, a reduction in the thermal gradient is observed, with air temperatures ranging from below 21 °C to 30 °C. The lowest temperatures (<21 to 22.5 °C) were associated with vegetated areas and cultivated fields, especially those located farther from the consolidated urban fabric. Intermediate values were representative of urban expansion zones (rural-urban transition) and patches of dense arboreal vegetation embedded within more densely built-up intra-urban areas. The highest temperatures, in turn, were linked to the consolidated urban area, with the warmest thermal range (27 to 30 °C) concentrated in portions of the city center.

This thermal pattern shows similarities to the previous episode, while also reflecting seasonal characteristics through the greater cooling observed in rural surroundings and vegetated areas. This can be attributed to higher relative humidity conditions during this period compared to September episodes, which contribute to lower energy absorption and enhanced cooling, ultimately modulating local-scale temperature variation.

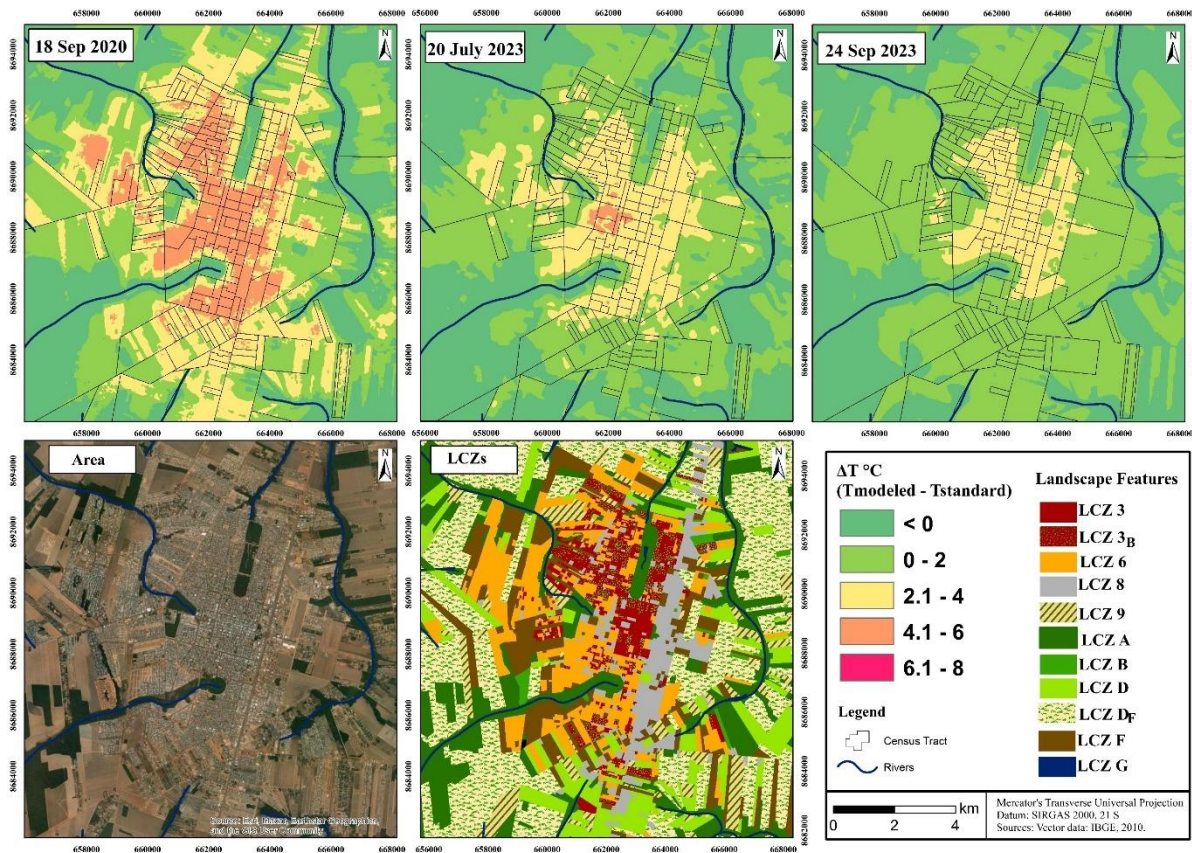
The temperatures observed for the 24 September model indicate a more widespread warming across the entire analytical area, with values predominantly ranging between 24 °C and 33 °C, presenting a markedly different scenario from the other episodes. Although present, the lowest temperature range in this episode (22.5 °C to 24 °C) was associated with dense arboreal vegetation located outside the intra-urban fabric and farther from built-up areas. Arboreal vegetation within the intra-urban area and its immediate surroundings was associated with slightly higher temperatures, between 24 °C and 25.5 °C, values noticeably higher than those recorded in the other two episodes.

Urban expansion areas, characterized by LCZs F, D_F, and 6, as well as the consolidated urban fabric (LCZs 3, 3_B, 8, and 6), and the surroundings of intra-urban arboreal vegetation predominantly recorded temperatures between 25.5 °C and 27 °C.

As indicated in the mobile transect analyses, this episode is representative of prolonged drought conditions and the influence of an atmospheric blocking pattern, which triggered a heatwave over the study area. Consequently, low relative humidity, even during nighttime hours, combined with clear-sky conditions and energy retention in the atmosphere, contributed to the thermal homogenization between urban and rural areas, with only subtle variations observed at specific points, typically associated with forest fragments. This highlights, in a localized manner, the relationship between the local climate and the dynamics of atmospheric circulation on a regional scale, as pointed out by Amorim (2020).

Finally, in order to qualitatively present the spatialization of the urban heat island in Sinop, Figure 11 is proposed, which contains the spatialization of the heat island intensities at 21:00h (local time) based on the values of modeled temperature. It is noteworthy that the standard temperature was selected in the pixel coinciding with the rural point (RP), located in the SW direction from the urban fabric, for the standardization of results and due to the fact that the $\Delta T^{\circ}\text{C}$ (modeled temperature - measured temperature) was lower than 1 °C.

Figure 11
Spatialization maps of urban heat island intensities, derived from the temperatures modeled for September 18, 2020; July 20, 2023; and September 24, 2023, at 21:00h, and their corresponding LCZs



Based on Figure 11, a preliminary comparison between the episodes highlights a reduction in the highest intensities characterizing stronger magnitudes ($\Delta T = 4.1$ to 6°C), particularly associated with the 2023 episodes. This change in the spatial pattern does not necessarily indicate that the city has cooled over time or that rural areas have significantly warmed. Rather, it reflects the seasonal characteristics of the episodes, which influence the spatial distribution of the heat island, even though all episodes represent the dry season, which in the study area extends from May to September.

While a change in the spatialized intensities is observed, spatial patterns remain similar. The first point to note is that the highest intensities in each episode are primarily associated with the consolidated urban fabric, corresponding to strong magnitude for September 18, 2020, and moderate for July 20 and September 24, 2023. These results are linked to landscape characteristics such as LCZs 3, 3_B, 6, and 8.

It is noteworthy that this spatial pattern of greater warming in the urban core, characterized by higher built density, has also been observed in other cities within the Amazonian context, even under different spatial scales, as reported by Aleixo et al. (2021) and Almeida Filho, Aleixo, and Silva Neto (2022). This highlights the role of these cities in altering the local climate in response to urban space production, as well as the homogenizing nature of capitalist urban development in the context of urban climate.

In contrast, urban expansion areas and rural surroundings show intermediate temperature differences for each episode, associated with landscape characteristics, such as LCZs 9, D_F, and F. The lowest thermal differences, particularly those below 0 °C, are associated with dense tree vegetation, forming “cold islands” when located within the intra-urban area, caused by evapotranspiration and latent heat dissipation, as verified in Dubreuil et al. (2024).

In summary, the spatializations of the modeled temperature and intensities confirm the changes in the thermal structure at the local scale as a function of the landscape properties and characteristics and the physical aspects of Sinop, with the built areas being the greatest influencers on the climatic component of the air temperature. The results also reflect the nature of these relationships under different conditions within the same seasonal period (dry season).

It also highlights the ability of agricultural activities, which are the main focus of the study area, to influence physical mechanisms, such as the energy flow, being represented in the identification of different results when compared to other rural characteristics, such as dense arboreal vegetations. These areas (LCZ D_F) were warmer than the vegetation, but less heated than the intra-urban areas.

Together with these observations, the importance of the role played by arboreal vegetation in controlling the distribution of the temperature of the modeled area is also highlighted, not only in rural surroundings, but also in forest fragments and in intra-urban areas.

Finally, it is noteworthy that the results observed are corroborated by studies in tropical cities, such as the one by Dorigon and Amorim (2019), who verified greater heating of LCZs that are characteristic of urban areas, such as LCZ 3 and LCZ 3_B, and smaller for rural LCZs or with low built density – such as LCZ 9 and LCZ A, among others. These results also corroborate Cardoso et al. (2017), Dorigon and Amorim (2019), Amorim (2020), and Ortiz Porangaba et al. (2021), Aleixo et al. (2021) and Almeida Filho, Aleixo, and Silva Neto (2022), among others, who observed greater heating of built areas as a function of their characteristics and the role played by vegetation as a mitigator of potential problems such as urban heat islands.

4. Final considerations

The results and validation parameters confirm the feasibility of analyzing urban heat islands through spatial modeling using multiple linear regression. The models highlight the influence of landscape properties and characteristics (LCZs), physical elements (NDVI), and aspects of urban spatial organization (e.g., distance from the city center and arboreal vegetation) on air temperature.

The spatialization of air temperature and heat island intensity reinforced patterns identified in previous studies (Cardoso & Amorim, 2018; Xiao et al., 2018; Choudhury et al., 2021; Ortiz Porangaba et al., 2021; Gao et al., 2022). Areas with dense arboreal vegetation consistently presented lower temperature values and intensities, particularly when located away from built-up areas, thus standing out as priority zones for identifying cool islands.

In contrast, the consolidated urban fabric was characterized by recurring zones of moderate to very strong heat island magnitudes.

Furthermore, areas used for seasonal crops (LCZ D_F) were identified as less heated than the urban fabric, yet warmer than arboreal vegetation zones, suggesting the role of socioeconomic activities in shaping the spatial organization of local climate elements.

It is noteworthy that, although the number of episodes and their temporal coverage are limited, the seasonal atmospheric characteristics of the dates selected in this study reinforce the representativeness and features of the urban heat island during the dry periods. This finding can be validated through studies dedicated to the temporal analysis of the heat island in Sinop, such as those by Zavitoski (2018), Araújo (2021), and Dubreuil et al. (2024), among others. Therefore, it can be stated that the study does not present significant limitations, given the high representativeness of the analyzed episodes.

Finally, the results presented here also reinforce the importance of conducting comprehensive analyses within the same seasonal period (dry or rainy), as regional atmospheric circulation patterns influence the behavior of the urban climate. This broader understanding contributes to more accurate interpretations of the phenomenon and supports the development of more effective mitigation and adaptation strategies.

Informação Suplementar

Autores

Luis Flávio de Araújo – Programa de Pós-Graduação em Geografia, Universidade Estadual Paulista (Unesp), Faculdade de Ciências e Tecnologia, Presidente Prudente, São Paulo, Brasil
lf.araujo@unesp.br
ORCID: <https://orcid.org/0000-0002-2698-8091>

Margarete Cristiane de Costa Trindade Amorim – Universidade Estadual Paulista (Unesp), Faculdade de Ciências e Tecnologia, Presidente Prudente, São Paulo, Brasil
margarete.amorim@unesp.br
ORCID: <https://orcid.org/0000-0002-3975-493X>

Vincent Dubreuil – LETG-Rennes-COSTEL, Université Rennes 2, Rennes, França
damien.arvor@univ-rennes2.fr
ORCID: <https://orcid.org/0000-0001-8383-805X>

Financiamento:

Processo FAPESP n° 2021/08670-1
CAPES/COFECUB - processo: 88881.191765/2018-01; Sh 941/19 – projeto: CiCIAMEN (Cidades, Clima e Vegetação: Modelagem e Políticas Públicas Ambientais)

Nota

O presente artigo apresenta resultados parciais da Dissertação de mestrado intitulada: “**Ilhas de calor em Sinop: análise das características térmicas em conjunto com os aspectos socioeconômicos e ambientais**” e da Tese de Doutorado intitulada: “**Clima urbano e saúde: análise da correlação entre ilha de calor, concentração de MP₁₀ e espacialização de casos de doenças respiratórias em Sinop (MT)**”.

Data de submissão: 2025-07-11

Data de aceitação: 2025-11-12

Data de publicação: 2025-12-31

References

- Aleixo, N. C. R., Silva Neto, J. C. A., Alves, C. S., & Figueira Filho, A. (2021). Ilhas de calor em cidade de pequeno porte na Amazônia brasileira: Análise de Uarini-AM. *Revista Georaguuaia*, 11(Especial), 166-186. <https://periodicoscientificos.ufmt.br/ojs/index.php/geo/article/view/12072>
- Almeida Filho, L. S., Aleixo, N. C. R., & Silva Neto, J. C. A. (2022). Ilhas de calor urbanas na cidade de Coari-AM. *Revista GeoAmazônia*, 10(20), 116-134. <https://doi.org/10.18542/geo.v10i20.13661>
- Amorim, M. C. C. T. (2005). Intensidade e forma da ilha de calor urbana em Presidente Prudente/SP: Episódios de Inverno. *Geosul*, 20(39), 65-82. <https://periodicos.ufsc.br/index.php/geosul/article/view/13307>
- Amorim, M. C. C. T. (2020). *Ilhas de calor em cidades tropicais de médio e pequeno porte: teoria e prática*. Appris, Curitiba.
- Amorim, M. C. C. T., Dubreuil, V.; & Amorim, A. T. (2021). Day and night surface and atmospheric heat islands in a continental and temperate tropical environment. *Urban Climate*, 38, 100918. <https://doi.org/10.1016/j.uclim.2021.100918>
- Amorim, M. C. C. T., Dubreuil, V., & Cardoso, R. S. (2015). Modelagem espacial da ilha de calor urbano em Presidente Prudente (SP) - Brasil. *Revista Brasileira de Climatologia*, 16, 29-45. <http://dx.doi.org/10.5380/abclima.v16i0.40585>
- Araújo, L. F. (2021). *Ilhas de calor em Sinop: análise das características térmicas em conjunto com os aspectos socioeconômicos e ambientais* (Dissertação de Mestrado), Universidade Estadual Paulista, Faculdade de Ciências e Tecnologia, Presidente Prudente, Brasil. <https://hdl.handle.net/11449/213831>
- Araújo, L. F., Amorim, M. C. C. T., Dubreuil, V., & Arvor, D. (2022). A variação espacial da ilha de calor e sua associação com as características paisagísticas em Sinop-MT. *Revista Brasileira de Climatologia*, 31(18), 384-412. <https://doi.org/10.55761/abclima.v31i18.15470>
- Becker, B. (2001). Revisão das políticas de ocupação da Amazônia: É possível identificar modelos para projetar cenários? In Brasil, Ministério da Ciência e Tecnologia, Parcerias Estratégicas (n° 12). Brasília, Centro de Estudos Estratégicos (MCTI).
- Brasil (1980). Departamento Nacional de Produção Mineral. *Projeto RADAMBRASIL – Folha SC.21, Juruena: geologia, geomorfologia, pedologia, vegetação e uso potencial da terra*. DNPM, Rio de Janeiro.
- Cardoso, R. S., Dorigon, L. P., Teixeira, D. C. F., & Amorim, M. C. C. T. (2017). Assessment of urban heat islands in small- and mid-sized cities in Brazil. *Climate*, 5(14). <https://doi.org/10.3390/cli5010014>
- Cardoso, R. S., & Amorim, M. C. C. T. (2018). Urban heat island analysis using the ‘local climate zone’ scheme in Presidente Prudente, Brazil. *Investigaciones Geográficas*, 69, 107-118. <https://doi.org/10.14198/INGEO2018.69.07>
- Choudhury, D., Das, A., & Das, M. (2021). Investigating thermal behavior pattern (TBP) of local climatic zones (LCZs): A study on industrial cities of Asansol-Durgapur development area (ADDA), eastern India. *Urban Climate*, 35, 100727. <https://doi.org/10.1016/j.uclim.2020.100727>
- Clairay, M., & Dubreuil, V. (2002). Etude de l'évolution diachronique de la GlebaCeleste (Mato Grosso) à partir d'images Landsat. *Espaço e Geografia*, 5(1), 119-138. <http://www.lsie.unb.br/espacoegografia/index.php/espacoegografia/article/view/18>
- Dorigon, L. P.; & Amorim, M. C. C. T. (2019). Spatial modeling of an urban Brazilian heat island in a tropical continental climate. *Urban Climate*, 28, 100461. <https://doi.org/10.1016/j.uclim.2019.100461>
- Dorigon, L. P., & Amorim, M. C. C. T. (2020). Variabilidade espacial da temperatura do ar com uso de transectos móveis em

- Jundiá/SP. *Revista Brasileira de Climatologia*. 27, 349-367. <http://dx.doi.org/10.5380/abcclima.v27i0.73202>
- Dubreuil, V., Arvor, D., Nedelec, V., Nabucet, J., Brabant, C., Silva Júnior, C. A., Della Silva, J. L., Vendrusculo, L., Cardoso, B., Camillo de Carvalho, M. A., Rizzi, T., Bonini, I., Araújo, L. F., & Amorim, M. C. C. T. (2024). As ilhas de calor urbanas nas cidades da frente pioneira da Amazônia Mato-Grossense. In M. C. C. T. Amorim & V. Dubreuil (Eds.), *Cidades, clima e vegetação: modelagem e políticas públicas ambientais* (pp. 139–152). TotalBooks. <https://doi.org/10.52632/978.65.88393.62.8>.
- Dubreuil, V., Nedelec, V., Bariou, R., & Maitelli, G. T. (2003). Estudo da urbanização e suas consequências sobre as temperaturas noturnas em Sinop/Mato Grosso. *Revista Mato-grossense de Geografia*. 07/08, 25-39.
- Dubreuil, V., Delahaye, C., & Le Strat, A. (2010). Changements d'occupation du sol et leurs impacts climatiques au Mato Grosso, Brésil. *Confins*. 10, 6845. <https://doi.org/10.4000/confins.6845>
- Dubreuil, V., Fante, K. P., Planchon, O., & Sant'Anna Neto, J. L. (2018). Climate change evidence in Brazil from Koppen's climate annual types frequency. *International Journal of Climatology*, 1, 1-14. <https://doi.org/10.1002/joc.5893>
- Fernández García, F. (1996). *Manual de climatología aplicada: clima, medio ambiente y planificación*. Editorial Síntesis.
- Foissard, X. (2015). *L'îlot de chaleur urbain et le changement climatique : application à l'agglomération rennaise* [Doctoral thesis]. Université Rennes II, Rennes, France.
- Foissard, X., Dubreuil, V., & Quénel, H. (2019). Defining scales of the land use effect to map the urban heat island in a mid-size European city: Rennes (France). *Urban Climate*. 29, 100490. <https://doi.org/10.1016/j.uclim.2019.100490>
- Gao, Y., Zhao, J., & Han, L. (2022). Exploring the spatial heterogeneity of urban heat island effect and its relationship to block morphology with the geographically weighted regression model. *Sustainable Cities and Society*. 76, 103431. <https://doi.org/10.1016/j.scs.2021.103431>
- Gartland, L. (2010). *Ilhas de Calor: como mitigar zonas de calor em áreas urbanas*. Oficina de textos, São Paulo.
- IBGE (2022). Instituto Brasileiro de Geografia e Estatística. IBGE Cidades 2018. <https://cidades.ibge.gov.br/>
- Levin, J. (1977). *Estatística aplicada a ciências humanas*. HARBRA.
- Monteiro, C. A. F. (1975). *Teoria e clima urbano* [Habilitation thesis]. Universidade de São Paulo.
- Oke, T.R., Mills, G., Christen, A., & Voogt, J. A. 2017. *Urban Climates*. Cambridge University Press.
- Ortiz Porangaba, G. F., Teixeira, D. C. F., Amorim, M. C. C. T., Silva, M. H. S., & Dubreuil, V. (2021). Modeling the urban heat island at a winter event in Três Lagoas, Brazil. *Urban Climate*. 37, 100853. <https://doi.org/10.1016/j.uclim.2021.100853>
- Pinton, L. G., Ribeiro, M. C. A., Suizu, T. M., & Amorim, M. C. C. T. (2021). Magnitudes do fenômeno da ilha de calor urbana em Sacramento (MG): perspectivas de aplicação do sistema das Zonas Climáticas Locais em cidades de pequeno porte. *Caminhos de Geografia*. 22(79), 161-179. <https://doi.org/10.14393/RCG227953890>
- Pitton, S. E. C. (1997). *As cidades como indicadores de alterações térmicas* (Tese de doutorado). Universidade de São Paulo, São Paulo, Brasil.
- Stewart, I. D. (2011). *Redefining the urban heat island* (Doctoral thesis). The University of British Columbia, Vancouver, Canadá.
- Stewart, I. D., & Oke, T. R. (2012). Local Climate Zones for urban temperature studies. *BAMS*. 93(12), 1879-1900. <https://doi.org/10.1175/BAMS-D-11-00019.1>
- Xiao, X. D., Dong, L., Yan, H., Yang, N., & Xiong, Y. (2018). The influence of the spatial characteristics of urban green space on the urban heat island effect in Suzhou Industrial Park. *Sustainable Cities and Society*. 40, 428-439. <https://doi.org/10.1016/j.scs.2018.04.002>
- Yin, C., Yuan, M., Lu, Y., Huang, Y., & Liu, Y. (2018). Effects of urban form on the urban heat island effect based on spatial regression model. *Science of The Total Environment*, 634, 696-704. <https://doi.org/10.1016/j.scitotenv.2018.03.350>
- Zavitoski, E. V. S. (2018). *Análise termohigrométrica nos eixos viários centrais da malha urbana original de Sinop-MT* [Doctoral thesis]. Universidade Federal de Mato Grosso, Sinop, Brasil.
- Zheng, Z., Ren, G., Wang, H., Dou, J., Gao, Z., Duan, C., Li, Y., Ngarukiyimana, J. P., Zhao, C., Cao, C., Jiang, M., & Yang, Y. (2018). Relationship Between Fine-Particle Pollution and the Urban Heat Island in Beijing, China: Observational Evidence. *Boundary-Layer Meteorol*. 169, 93-113. <https://doi.org/10.1007/s10546-018-0362-6>